analytical chemistry

pubs.acs.org/ac Article

Structurally Engineered Light-Responsive Nanozymes for Enhanced Substrate Specificity

Yufeng Liu, Xiaoyu Wang, Quan Wang, Yihong Zhang, Quanyi Liu, Shujie Liu, Sirong Li, Yan Du, and Hui Wei*

Cite This: *Anal. Chem.* 2021, 93, 15150−15158 Read Online

ACCESS | Metrics & More | Article Recommendations | Supporting Information

ABSTRACT: Mimicking enzyme specificity via construction of on-demand geometric structures on nanozymes is of great interest in recent years. Although building substrate-specific polymers on nanozymes has achieved great success, polymer-blocked active sites would inevitably lead to decreased activity of nanozymes. Here, we have developed three photoactive metal−organic framework (MOF)-based nanozymes (called 2D-TCPP, 3D-TCPP, and AD-TCPP), which have different geometric structures as well as unshielded active sites. Together with their structural variations and excellent photoresponsive oxidase-like activities, these photoactive nanozymes exhibit structure-dependent specificity for three kinds of substrates (typical oxidase substrates, organic pollutants, and antioxidants). Moreover, AD-TCPP and 3D-TCPP show potential applications for environmental protection and bioanalysis, respectively. This work offers a promising approach to the development of nanozymes with enzyme-like specificity.

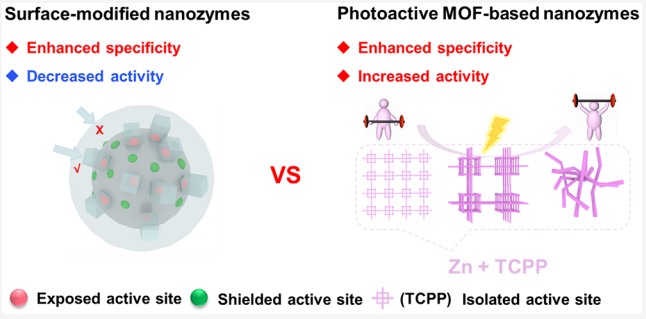

INTRODUCTION

Catalytic specificity is one of the most attractive features of natural enzymes, playing a vital role in the metabolisms and transformations of organism.[1] To utilize such a fantastic property for enhancing on-demand substrate selectivity, numerous efforts have been devoted toward it, such as enzyme engineering and enzyme immobilization.[2−4] However, due to the inherent limitations of natural enzymes, such as low stability in nonphysiological environments, high cost of production, and difficulty in storage, the regulation of enzyme specificity remains a prominent and ongoing challenge. To this end, we reasoned that using artificial enzymes to replace natural enzymes for the design of substrate specificity is of great significance because of their stable, rich, and diverse structures. Among artificial enzymes, nanomaterials with enzyme-like activities (called nanozymes) are attracting increasing attention owing to their unique features including flexible designability, tunable activity, and multifunctionalities.[5−9]

The substrate specificity of natural enzymes usually comes from the distinct combinations of amino acids that facilitates the diffusion and binding of specific substrates to catalytically active sites. Previous studies have shown that the construction of substrate binding pocket-like structures on catalytic active sites is a promising method to enhance substrate specificity.[10−13] Accordingly, growing polymeric shells with substrate selectivity on nanozymes is a prevalent method for the fabrication of specific nanozymes. For instance, the Liu group has applied the molecular imprinting strategy on Fe_3O_4 nanozyme and the as-constructed peroxidase mimics exhibited significant specificity for 3,3′,5,5′-tetramethylbenzidine dihydrochloride (TMB) and 2,2′-azinobis (3-ethylbenzothiazoline-6-sulfonic acid) ammonium (ABTS).[14] Although this proof-of-concept work has achieved a significant substrate specificity, a lot of external active sites on Fe_3O_4 nanozyme are inevitably blocked by the imprinted polymers. Because of the blocked active sites, such a specific nanozyme needs a long reaction time and a high concentration of H_2O_2, which in turn limits its potential applications. In general, the surface coating strategy for enhancing substrate selectivity of nanozymes unavoidably faces the shortage of shielded active sites. Therefore, new strategies to develop specific nanozymes with unshielded active sites are greatly needed. To this end, we reasoned that metal−organic frameworks (MOFs) with flexible porous structures and efficient mass transfer capabilities could be used as an ideal model to develop nanozyme's specificity.[15−18]

Recently, the use of light as an external stimulus has been demonstrated as a facile, controllable, and effective method for modulating activity of nanozymes.[19,20] Several light-responsive

Received: August 22, 2021
Accepted: October 22, 2021
Published: November 5, 2021

https://doi.org/10.1021/acs.analchem.1c03610
Anal. Chem. 2021, 93, 15150−15158

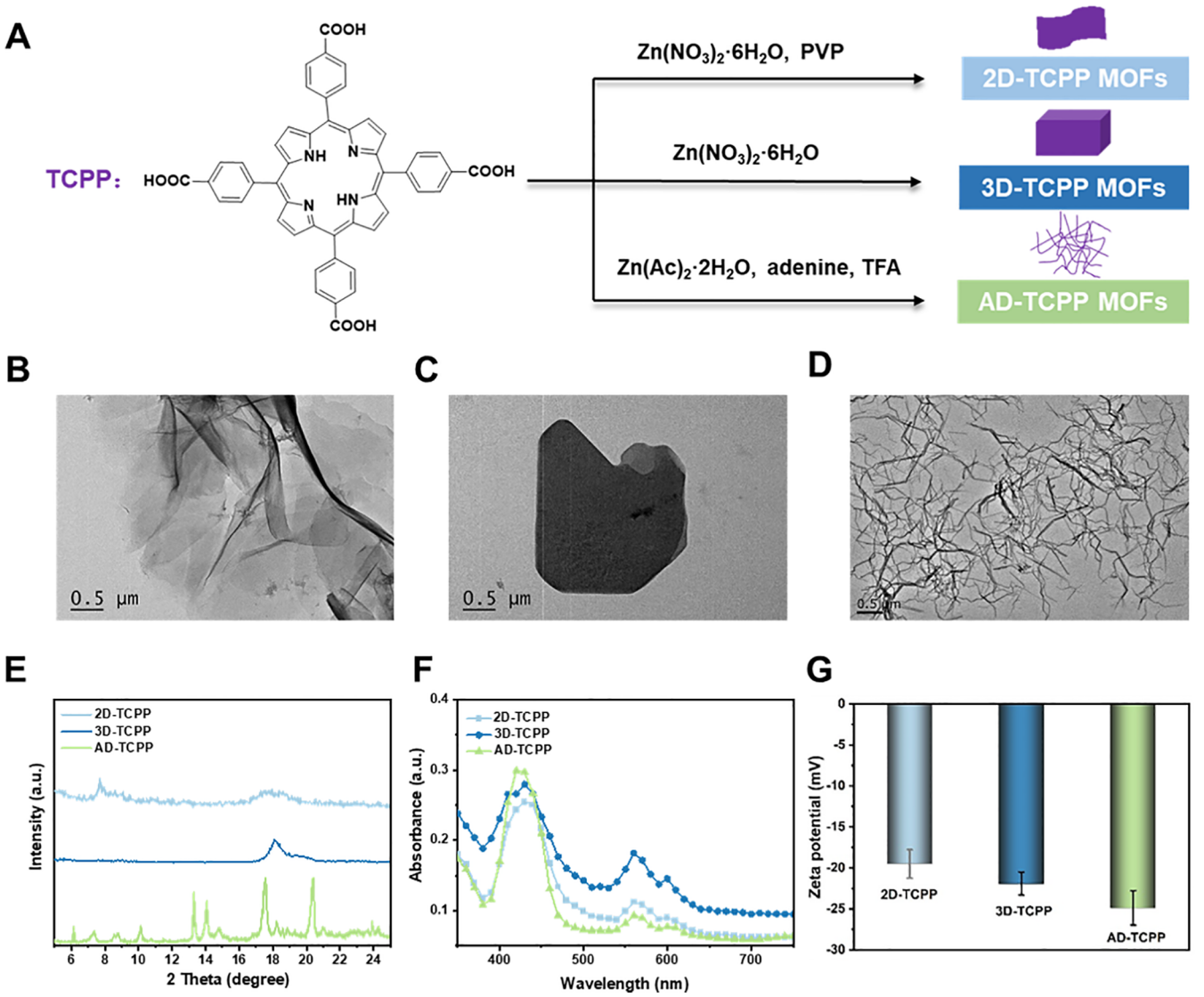

Figure 1. (A) Synthesis procedures of 2D-TCPP, 3D-TCPP, and AD-TCPP. TEM images of 2D-TCPP (B), 3D-TCPP (C), and AD-TCPP (D). (E) PXRD patterns of 2D-TCPP, 3D-TCPP, and AD-TCPP. (F) UV−visible absorption spectra of 2D-TCPP, 3D-TCPP, and AD-TCPP. (G) ζ Potentials of 2D-TCPP, 3D-TCPP, and AD-TCPP. Each error bar shows the standard deviation of three independent measurements.

nanozymes with excellent enzyme-like activities have been successfully applied in bioanalysis, environment protection, and biomedicine.[21−23] However, none of them has been focused on the substrate specificity. Considering that photoresponsive MOF nanozymes have both adjustable structure and excellent oxidase-like activity, it would be a promising strategy to structurally engineer photoresponsive MOF nanozymes for enhancing the substrate specificity.

Herein, we synthesized three photoactive MOF nanozymes with different structures (designated as two-dimensional (2D)-TCPP, three-dimensional (3D)-TCPP, and adenine (AD)-TCPP, respectively). Taking advantage of their excellent photoresponsive oxidase-like activities, we reacted them with a variety of substrates (typical oxidase substrates, organic pollutants, and antioxidants) and tried to elucidate a potential structure−substrate selectivity relationship. We found that 2D-TCPP nanozyme has the fastest reaction rate for TMB and ABTS but the lowest for *o*-phenylenediamine (OPD); AD-TCPP nanozyme has the best degradation efficiency for methylene blue (MB) than methyl orange (MO), rhodamine 6G (Rh6G), and neutral red (NR); and only 3D-TCPP nanozyme shows the best discrimination against six kinds of antioxidants.

RESULTS AND DISCUSSION

Synthesis and Characterization of 2D-TCPP, 3D-TCPP, and AD-TCPP. We selected meso-tetra(4-carboxyphenyl) porphine (TCPP), a typical photoactive molecule, for synthesizing MOFs with different structures. As shown in Figure 1A, using several facile methods, we have synthesized three MOFs (*i.e.*, 2D-TCPP, 3D-TCPP, and AD-TCPP) with structures of sheet, bulk, and wire. Transmission electron microscopic (TEM) imaging in Figures 1B−D and S1 confirmed their successful formations. The powder X-ray diffraction (PXRD) patterns in Figure 1E showed the characteristic peaks of 2D-TCPP, 3D-TCPP, and AD-TCPP, demonstrating their good crystallinities. UV−visible absorption spectra showed that all of these MOFs had the characteristic peaks of TCPP, which were at 430, 560, and 600 nm, endowing them with potential photoactive abilities (Figure

https://doi.org/10.1021/acs.analchem.1c03610
Anal. Chem. 2021, 93, 15150−15158

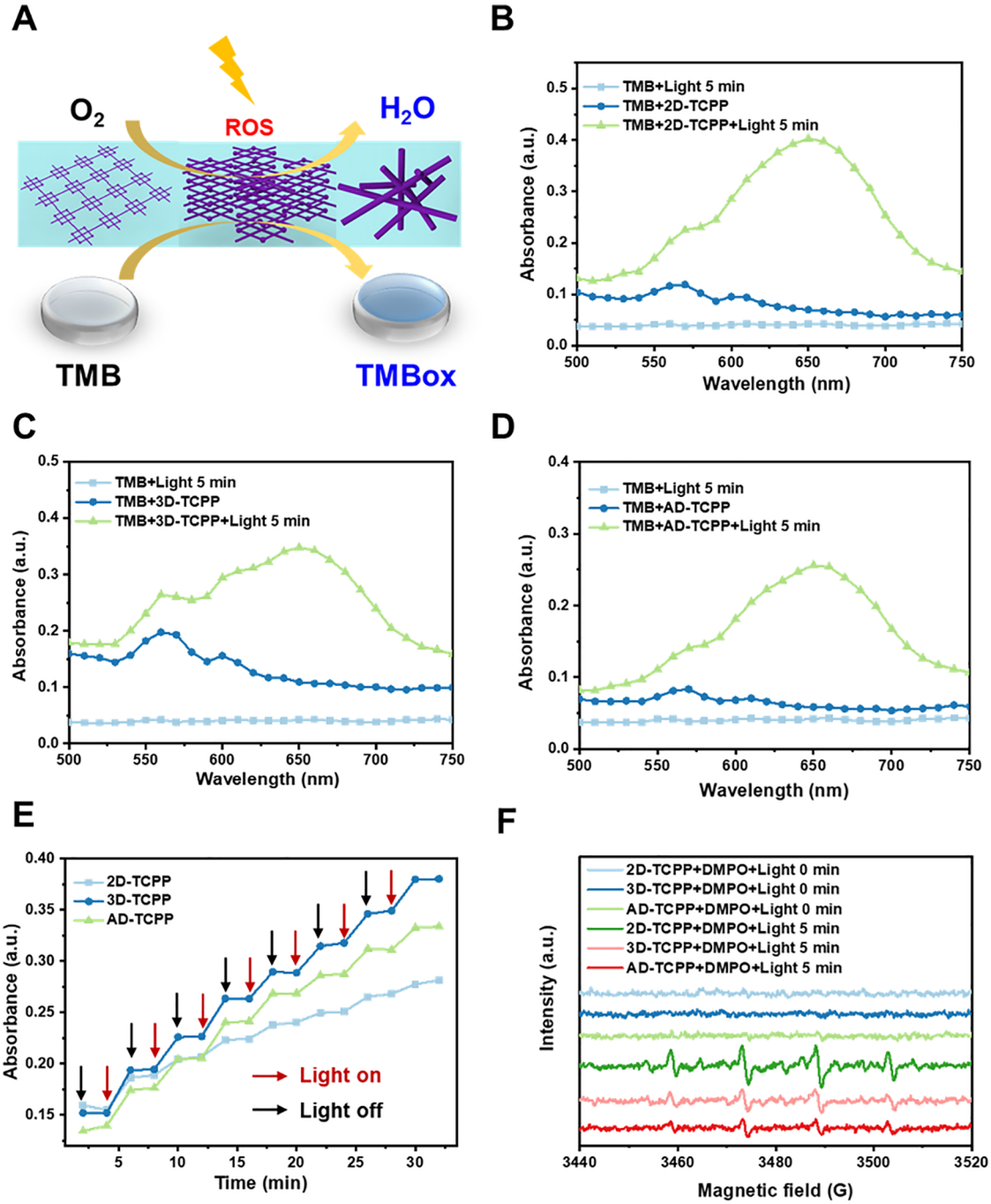

Figure 2. (A) Schematic illustration of the photoresponsive catalysis. (B) UV−vis absorption spectra of three samples in 0.1 M acetate buffer (pH 4.5) containing TMB (under light irradiation), 2D-TCPP + TMB (no light irradiation), and 2D-TCPP + TMB (under light irradiation). (C) UV−vis absorption spectra of three samples in 0.1 M acetate buffer (pH 4.5) containing TMB (under light irradiation), 3D-TCPP + TMB (no light irradiation), and 3D-TCPP + TMB (under light irradiation). (D) UV−vis absorption spectra of three samples in 0.1 M acetate buffer (pH 4.5) containing TMB (under light irradiation), AD-TCPP + TMB (no light irradiation), and AD-TCPP + TMB (under light irradiation). (E) Staircase-like behavior of oxidase-like activity when the light source was turned on and off, indicated by reddish and black arrows, respectively. (F) EPR spectra of nanozymes (2D-TCPP, 3D-TCPP, and AD-TCPP) and DMPO mixed solution in the absence and presence of irradiation with a Xe lamp.

1F). Moreover, ζ potentials of 2D-TCPP, 3D-TCPP, and AD-TCPP were about −19, −21, and −24 mV (Figure 1G), indicating their similar electrostatic adsorption capabilities toward positively charged substrates.

Light-Responsive Oxidase-like Activities of 2D-TCPP, 3D-TCPP, and AD-TCPP. Then, light-responsive oxidase-like activities of these MOFs were evaluated using a typical oxidase chromogenic substrate TMB in 0.1 M acetate buffer (pH 4.5) (Figure 2A). UV−vis spectroscopy was applied to monitor the catalytic oxidation. As shown in Figure 2B, under light irradiation, the sample containing TMB alone showed no absorption peak at 652 nm, indicating that no oxidized TMB (TMB_{ox}) was produced. However, the sample containing 2D-TCPP and TMB showed a strong absorption peak of TMB_{ox} at

https://doi.org/10.1021/acs.analchem.1c03610
Anal. Chem. 2021, 93, 15150−15158

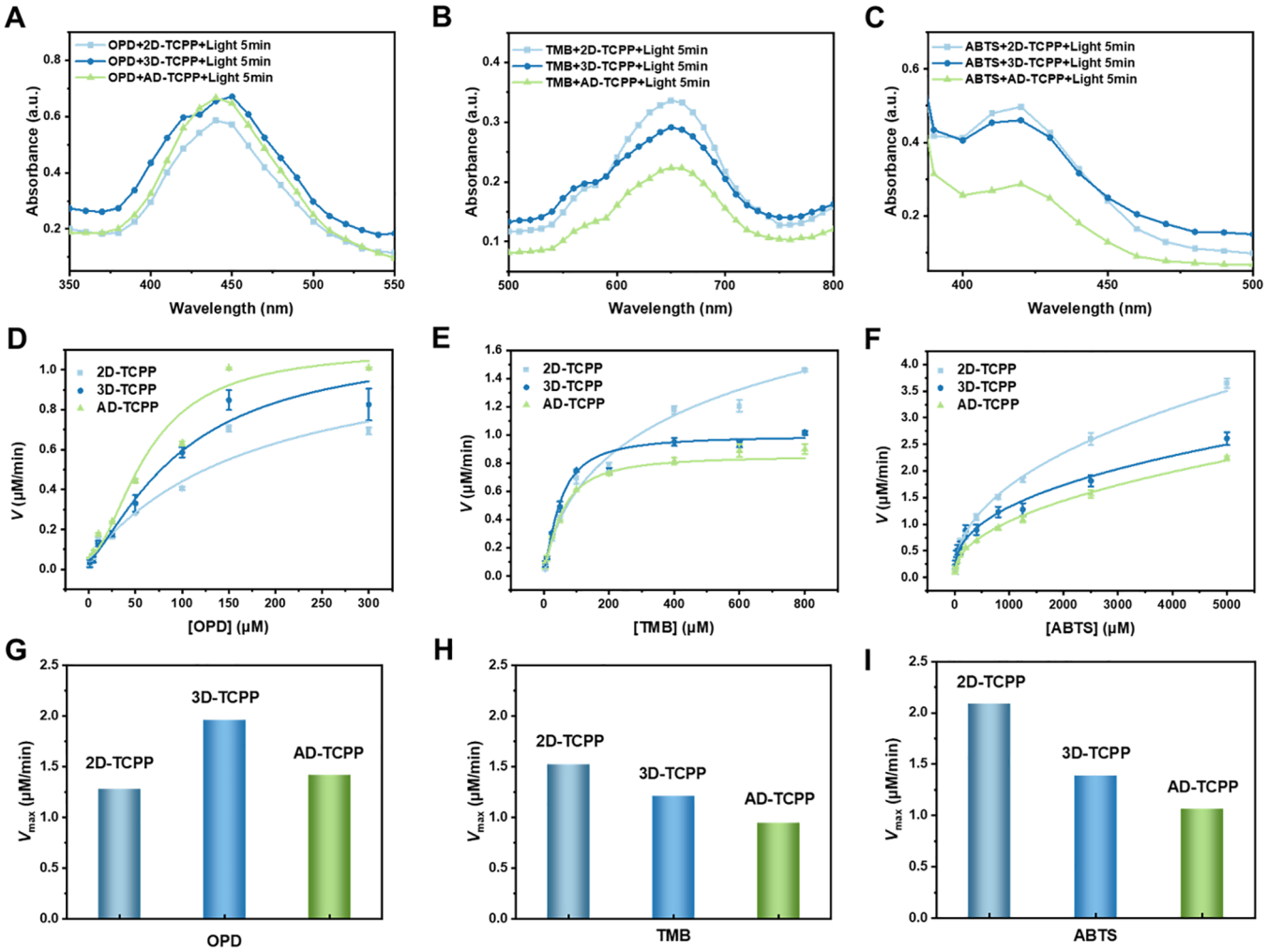

Figure 3. UV−visible absorption spectra of three samples in 0.1 M acetate buffer (pH 4.5) containing 2D-TCPP, 3D-TCPP, and AD-TCPP in the presence of (A) OPD, (B) TMB, and (C) ABTS, after irradiation for 5 min. Catalytic rates in the presence of various concentrations of (D) OPD, (E) TMB, and (F) ABTS substrates by 2D-TCPP, 3D-TCPP, and AD-TCPP. Comparison of the oxidase-like activities of the three nanozymes in terms of V_{max} toward substrates of (G) OPD, (H) TMB, and (I) ABTS. Each error bar shows the standard deviation of three independent measurements.

652 nm under light irradiation, which means that the 2D-TCPP exhibits a light-responsive oxidase-like activity. In contrast, there was almost no absorption peak at 652 nm of the same sample without irradiation, further confirming the stimuli-responsive activity of 2D-TCPP. Meanwhile, attributing to the same photoactive linker of TCPP, both 3D-TCPP and AD-TCPP showed excellent light-responsive oxidase-like activities (Figure 2C,D). Besides, by successively turning off and on the light irradiation, the oxidase-like activities of these MOFs exhibited staircase-like behaviors, indicating their efficient controllability (Figure 2E). Moreover, to identify the active species involved in the catalysis, electron paramagnetic resonance (EPR) was used to measure signals of 5,5-dimethyl-1-pyridine *N*-oxide (DMPO)-trapped reactive oxygen species (ROS). As shown in Figure 2F, all three light-responsive nanozymes exhibited typical EPR signals of DMPO-OOH, indicating that $^{\bullet}$OH was the main light-induced ROS.

Structure-Dependent Selectivity of Photoactive Nanozymes for Typical Oxidase Substrates. Although TMB, OPD, and ABTS are typical substrates for oxidases, the rates of reaction between them and oxidase could be different because of their distinct structures and sizes (Figure S2). It is necessary to measure the reaction rates of nanozymes for different kinds of substrates for better comparing their specificity. Therefore, the reaction rates of 2D-TCPP, 3D-TCPP, and AD-TCPP toward typical oxidase substrates were evaluated. As shown in Figure 3A−C, 3D-TCPP nanozyme showed a better oxidase-like activity for OPD than 2D-TCPP and AD-TCPP. Meanwhile, for TMB and ABTS, 2D-TCPP nanozyme exhibited higher activity than 3D-TCPP and AD-TCPP. The difference indicates that these photoactive nanozymes have a structure-dependent selectivity for OPD, TMB, and ABTS. In addition, for the steady-state kinetic study, Michaelis−Menten curves were obtained and kinetic parameters were calculated based on the equation: $V = V_{max}[S]/(K_m + [S])$, where V is the initial velocity, $[S]$ is the concentration of substrate, V_{max} is the maximum reaction velocity, and K_m is the Michaelis constant. As shown in Figure 3D−I and Table 1, 2D-TCPP nanozyme showed the highest V_{max} value for TMB and ABTS but the lowest for OPD.

On the other hand, according to our previous work, it is expected that the prepared 2D MOF nanozymes possess enhanced peroxidase-mimicking activities than their 3D bulk analogues since 2D structures have highly exposed surface area

https://doi.org/10.1021/acs.analchem.1c03610
Anal. Chem. 2021, 93, 15150−15158

Table 1. Comparison of the Kinetic Parameters of 2D-TCPP, 3D-TCPP, and AD-TCPP

	OPD	TMB	ABTS	
V_{max} (μM/min)	1.28	1.52	2.09	**2D-TCPP**
K_m (μM)	170	130	68	**2D-TCPP**
V_{max} (μM/min)	1.96	1.21	1.39	**3D-TCPP**
K_m (μM)	230	67	36	**3D-TCPP**
V_{max} (μM/min)	1.42	0.95	1.07	**AD-TCPP**
K_m (μM)	85	58	48	**AD-TCPP**

with more accessible active sites for enzymatic catalysis.[24] However, such superior performance was not observed in this work when using OPD as a substrate. Because of the relatively small size of OPD, the better oxidase-like activity of 3D-TCPP might be attributed to its pore confinement effect, which could locally load high amounts of OPD.[25,26]

Structure-Dependent Selectivity of Photoactive Nanozymes for Organic Pollutants. Nanozymes are advantageous over natural enzymes because they can also catalyze the reaction of nonenzyme substrates, such as organic pollutants.[27−29] To further evaluate the photoactive nanozymes' structure-dependent selectivity, several organic pollutants including cationic MB, anionic MO, anionic Rh6G, and NR have been selected as model substrates (Figure S4). Because of the electrostatic adsorption between the positively charged MB and the negatively charged nanozymes, AD-TCPP and 2D-TCPP showed the obvious degradation efficiencies of MB (Figure S5C). To our surprise, the negatively charged 3D-TCPP showed no response for MB, which was probably due to

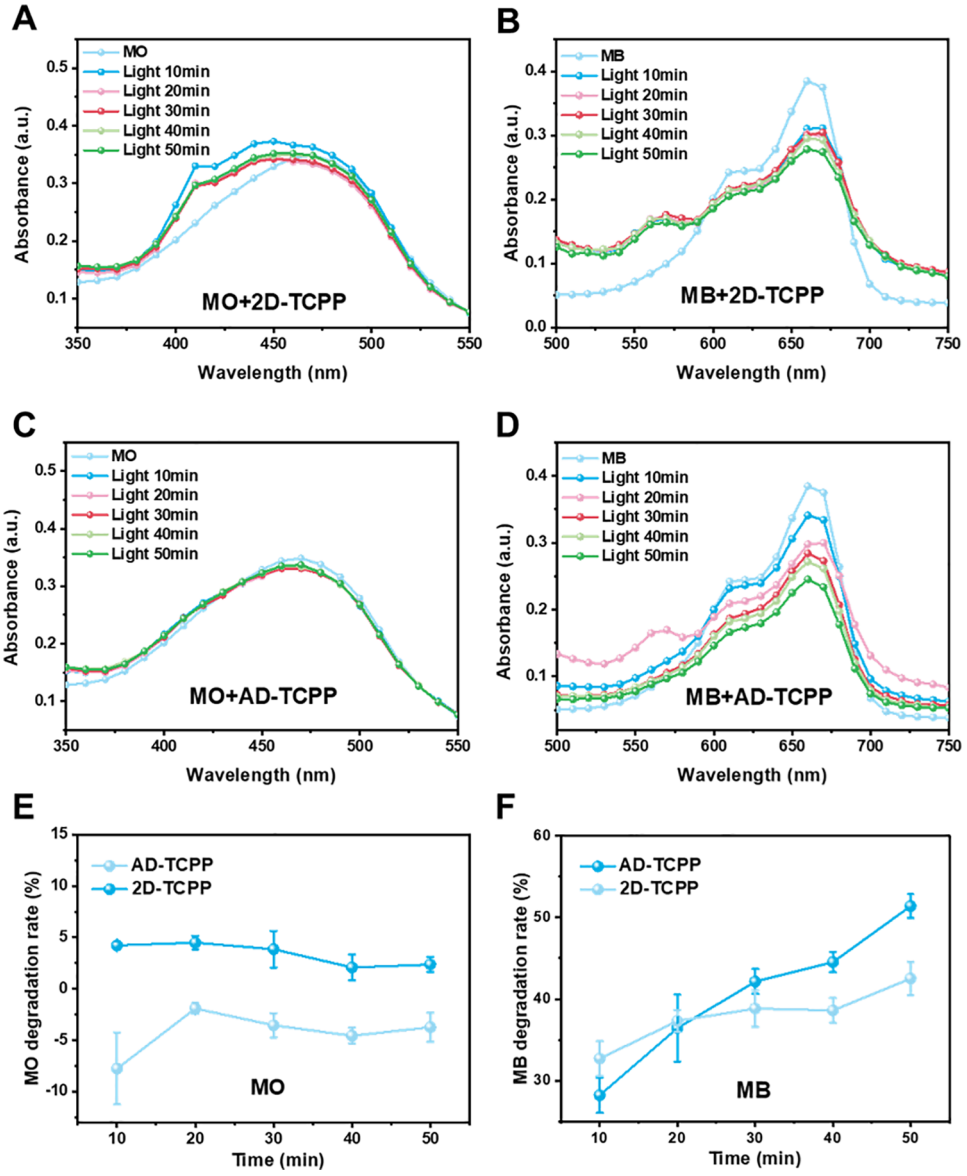

Figure 4. (A) UV−vis absorption spectra of samples containing MO and 2D-TCPP under different times of irradiation. (B) UV−vis absorption spectra of samples containing MB and 2D-TCPP under different times of irradiation. (C) UV−vis absorption spectra of samples containing MO and AD-TCPP under different times of irradiation. (D) UV−vis absorption spectra of samples containing MB and AD-TCPP under different times of irradiation. (E) Kinetic curves of the MO degradation rate in the presence of 2D-TCPP and AD TCPP under light irradiation. (F) Kinetic curves of the MB degradation rate in the presence of 2D-TCPP and AD TCPP under light irradiation. Each error bar shows the standard deviation of three independent measurements.

https://doi.org/10.1021/acs.analchem.1c03610
Anal. Chem. 2021, 93, 15150−15158

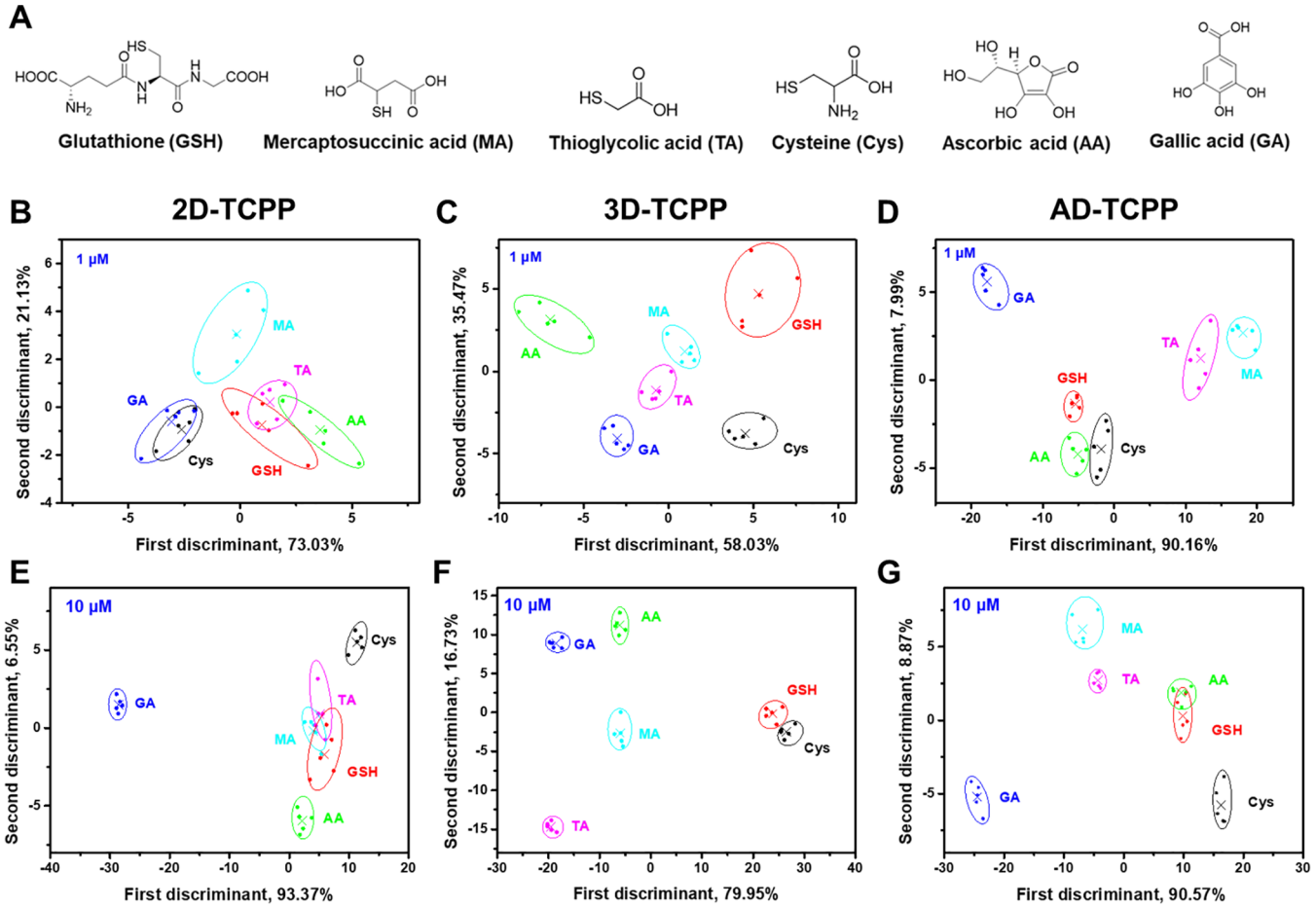

Figure 5. (A) Six kinds of antioxidants. 2D-TCPP (B), 3D-TCPP (C), and AD-TCPP (D) sensor arrays for discriminations against 1 μM of antioxidants. 2D-TCPP (E), 3D-TCPP (F), and AD-TCPP (G) sensor arrays for discriminations against 10 μM of antioxidants.

the limited interaction between them. The adsorption experiments of MB further demonstrate that 3D-TCPP has a poor adsorption capacity for MB, thus making it difficult to degrade MB (Figures S6 and S7). For other dyes, we found that the small-sized MO and NR could also be degraded by AD-TCPP or 2D-TCPP, while the large-sized Rh6G was difficult to be degraded by all of these photoactive nanozymes, indicating that the dimensions of dyes also affected their degrading rates (Figure S5A, S5B and Table S1). Although such a dimension effect was credible, the electrostatic effect obviously was more important for degrading rates among these organic dyes. Therefore, we aim to further evaluate the specific degradation of MB upon 2D-TCPP and AD-TCPP (MO was used as a negative control). As shown in Figure 4A−F, by measuring the time-dependent degradation rates, 2D-TCPP showed a higher degradation efficiency than AD-TCPP in the initial 10 min. However, with the increase of irradiation time, the degradation efficiency of AD-TCPP on MB gradually exceeds that of 2D-TCPP. One possible reason is that the structure of 2D-TCPP is unstable under long-term irradiation (Figure S8). Thus, we reason that AD-TCPP has the best degradation efficiency for MB.

Structure-Dependent Selectivity of Photoactive Nanozymes for Antioxidants. In addition to typical oxidase substrates and organic pollutants, antioxidants could act as substrates for nanozymes with oxidase- or peroxidase-like activities via the redox reactions. Given such redox mechanisms, detecting antioxidants using nanozyme-based colorimetric probes showed a promising way for disease diagnosis.[30−32] However, due to the limited specificity of nanozyme, it is still a challenge to selectively distinguish various antioxidants. Thus, using nanozymes with enhanced antioxidants specificity to discriminate them is of great significance. To evaluate these photoactive nanozymes' antioxidants specificity, we combined a photoactive nanozyme with three substrates (TMB, OPD, and ABTS) to construct a sensor array for discrimination of different antioxidants.

As shown in Figures 5A, S10, and S11, antioxidants including glutathione (GSH), mercaptosuccinic acid (MA), thioglycolic acid (TA), cysteine (Cys), ascorbic acid (AA), and gallic acid (GA) showed different signals on each sensor array. Analyzing these signals by linear discriminant analysis (LDA) could convert the training matrix into three canonical scores, and the first two most important discriminating factors could generate 2D canonical score plots. As shown in Figure 5B−D, for 1 μM antioxidants, 3D-TCPP- and AD-TCPP-based sensor arrays show better discriminations than 2D-TCPP, indicating that the 2D photoactive nanozyme has poor specificity for these antioxidants. Moreover, for 10 μM antioxidants, only the 3D-TCPP-based sensor array still maintains the full discrimination for each reducing molecule, which not only shows the best structure-dependent selectivity of 3D-TCPP but also provides a potential application for bioanalysis in future (Figure 5E−G). For this 3D-TCPP sensor array, the dynamic range of the antioxidant concentration is suitable from 0.1 to 100 μM (Figures S12 and S13). We reason that such a superior

https://doi.org/10.1021/acs.analchem.1c03610
Anal. Chem. 2021, 93, 15150−15158

discriminating capacity may originate from the pore confinement of 3D-TCPP, which is able to amplify the difference of pore diffusion rates for antioxidants with various sizes. However, for discriminations against two antioxidants (GSH and Cys) with different compositions, the 3D-TCPP sensor array can only distinguish samples containing 25% GSH + 75% Cys, 50% GSH + 50% Cys, and 75% GSH + 25% Cys. Because of the similar reducibility, samples containing 75% GSH + 25% Cys and 100% Cys cannot be fully distinguished with the 3D-TCPP sensor array (Figure S14).

CONCLUSIONS

In summary, we have developed three light-responsive nanozymes with excellent oxidase-like activities. The oxidase-like activity could be easily modulated by switching the "on/off" state of light. Using three types of substrates (typical oxidase substrates, organic pollutants, and antioxidants), we evaluated the structure-dependent selectivity of these photoactive nanozymes. Specifically, for typical oxidase substrates, 2D-TCPP shows the fastest reaction rate for TMB and ABTS but the lowest for OPD. For organic pollutants, AD-TCPP shows the fastest degrading rate for MB than for MO, Rh6G, and NR. For antioxidants, only 3D-TCPP-based sensor array shows the complete discrimination for each reducing molecule. It should be noted that the exact mechanisms of the nanozyme selectivity need to be elucidated in the future. Nevertheless, given the rapid development of nanozymes and versatile structure modulation of nanomaterials, this work could encourage us to develop nanozymes with enhanced substrate specificity by engineering the material dimension.

EXPERIMENTAL SECTION

Materials and Reagents. Commercially available reagents were of analytical grade and used without further purification. Meso-tetra(4-carboxyphenyl) porphine (TCPP) was purchased from Shanghai Macklin Biochemical Technology Co., Ltd. (Shanghai, China). Methyl orange, methylene blue, adenine, rhodamine 6G, mercapto acetic acid, gallic acid, mercaptosuccinic acid, zinc nitrate hexahydrate, 3,3′,5,5′-tetramethylbenzidine dihydrochloride (TMB), 2,2′-azinobis-(3-ethylbenzothiazoline-6-sulfonic acid) ammonium (ABTS), *N*,*N*-dimethylformamide (DMF), L-cysteine (L-Cys), and 5,5-dimethyl-1-pyridine *N*-oxide (DMPO) were purchased from Aladdin Chemical Co. Ltd. (Shanghai, China). Neutral red, zinc acetate, trifluoroacetic acid, ascorbic acid, and *o*-phenylenediamine (OPD) were purchased from Sinopharm Chemical Reagent Co. Ltd. (Shanghai, China). Glutathione (GSH) was obtained from J&K Scientific (Shanghai, China). Poly(vinylpyrrolidone) (PVP, MW = 24 000) was purchased from Sigma-Aldrich. All aqueous solutions were prepared with deionized water (18.2 MΩ·cm, Millipore).

Instrumentation. UV−visible absorption spectra were recorded on a UV−visible spectrophotometer with a 1 cm quartz cell (Purkinje General Instrument Co., Ltd., Beijing, China) and a microplate reader (SpectraMax M2e, Molecular Device Co., Ltd., San Jose). Transmission electron microscopic (TEM) imaging was performed on a Tecnai F20 microscope (FEI) at an acceleration voltage of 200 kV. Powder X-ray diffraction (PXRD) patterns were measured with an ARL SCINTAC X'TRA diffractometer using Cu Kα radiation (Thermo). ζ Potentials were measured on a Nanosizer ZS90 (Malvern). A 300 W Xe lamp with a filter above 400 nm was used for light irradiation (CEL-HXF300/CEL-HXUV300, China Education Au-light Co., Ltd., Beijing, China).

Synthesis of 2D MOF Nanozyme (2D-TCPP). 2D-TCPP was synthesized by following a previous procedure with minor revisions.[26] Typically, $Zn(NO_3)_2{\cdot}6H_2O$ (4.5 mg) and PVP (20 mg) were dissolved in 12 mL of a DMF−ethanol mixture (V/V = 3:1), followed by addition of 4 mL of DMF−ethanol mixture (V/V = 3:1) containing TCPP (4 mg). After that, the solution was sonicated for 10 min. The obtained reaction solution was then heated to 80 °C and kept for 24 h. The reaction mixture was cooled and centrifuged (8000 rpm, 10 min) to obtain purple precipitate, which was washed multiple times with ethanol. Finally, the obtained 2D-TCPP nanozymes were redispersed in DMF.

Synthesis of 3D MOF Nanozyme (3D-TCPP). 3D-TCPP was synthesized by following a previous procedure with minor revisions.[26] Typically, $Zn(NO_3)_2{\cdot}6H_2O$ (6 mg) and TCPP (8.8 mg) were dissolved in 2 mL of a DMF−ethanol mixture (V/V = 3:1) and sonicated for 10 min. The obtained reaction solution was then heated to 80 °C and kept for 24 h. The reaction mixture was cooled and centrifuged (8000 rpm, 10 min) to obtain purple precipitate, which was washed multiple times with ethanol. Finally, the obtained 3D-TCPP nanozymes were redispersed in DMF.

Synthesis of Adenine-Based MOF Nanozyme (AD-TCPP). AD-TCPP was synthesized by following a previous procedure with minor revisions.[33] Typically, zinc acetate (30 mg) and TCPP (42 mg) were dissolved in 7.5 mL of a DMF−H_2O mixture (V/V = 4:1), followed by addition of trifluoroacetic acid (30 drops). The obtained reaction solution was sealed in a 20 mL hydrothermal reactor, heated to 120 °C, and kept for 72 h. The reaction mixture was cooled and centrifuged (10 000 rpm, 10 min) to obtain a precipitate, which was washed three times with DMF. Finally, the obtained AD-TCPP nanozymes were redispersed in DMF.

Measurement of the Light-Responsive Oxidase-like Activity. NaOAc buffer solution (500 μL, 0.1 M) (pH 4.5) containing MOF-based nanozymes (20 μg/mL) and TMB (500 μM) was mixed. The mixed solution was illuminated using a 300 W Xe lamp with a filter above 400 nm for 5 min to activate the dissolved oxygen for oxidizing TMB. Subsequently, UV−vis absorption spectra were collected.

Electron Paramagnetic Resonance (EPR) Measurement. NaOAc buffer solution (200 μL, 0.1 M) (pH 4.5) containing MOF-based nanozymes (20 μg/mL) and DMPO (100 mM) was mixed. After being illuminated for 5 min, the mixture was characterized by a Bruker EMX-10/12 spectrometer operating at the X-band frequency (9.7 GHz) at room temperature.

Kinetics Assays. All steady-state kinetics assays were conducted at room temperature in 1.0 mL cuvettes with a path length of 1.0 cm. A 0.1 M NaOAc buffer solution (pH 4.5) was used as the reaction buffer. MOF-based nanozymes with final concentrations of 20 μg/mL were used for their kinetics assays. The kinetics measurements were carried out after illumination for 5 min. The kinetics data were obtained by varying the concentration of substrate (TMB, OPD, ABTS) while keeping the nanozyme's concentration constant. In the suitable concentration range of substrates, typical Michaelis−Menten curves were obtained.

Degradation of Organic Pollutants. In general, 500 μL of 0.1 M NaOAc buffer solution (pH 4.5) containing MOF-based nanozymes (20 μg/mL) and organic pollutant was

https://doi.org/10.1021/acs.analchem.1c03610
Anal. Chem. 2021, 93, 15150−15158

mixed. The mixed solution was irradiated using a 300 W Xe lamp with a filter above 400 nm for 50 min. The absorbance of the organic pollutant was collected every 10 min.

Discrimination of Antioxidants. Six kinds of antioxidants were detected as follows. NaOAc buffer solution (0.1 M, 1000 μL, pH 4.5) containing nanozyme (20 μg/mL), substrate (500 μM), and analytes (0.1, 0.5, 1, 5, 10, 50, 100, and 250 μM) was illuminated for 5 min. Then, reaction solutions (150 μL) were added into the wells of a 96-well plate to collect the absorbance. The six antioxidants were tested against three substrates five times to give a six antioxidants × three arrays × five replicates training data matrix. The raw data matrix was processed using linear discriminant analysis (LDA).

■ ASSOCIATED CONTENT

Supporting Information

The Supporting Information is available free of charge at https://pubs.acs.org/doi/10.1021/acs.analchem.1c03610.

TEM images, molecular formulas, absorption spectra, kinetic curves, SEM images, stability of MOFs under light illumination, dynamic range for the sensor array, Brunauer−Emmett−Teller (BET) measurements, comparisons of molecular dimensions between different dyes, and comparisons of BET surface areas between different MOFs (PDF)

■ AUTHOR INFORMATION

Corresponding Author

Hui Wei − *Department of Biomedical Engineering, College of Engineering and Applied Sciences, Nanjing National Laboratory of Microstructures, Jiangsu Key Laboratory of Artificial Functional Materials, Nanjing University, Nanjing, Jiangsu 210023, China; State Key Laboratory of Analytical Chemistry for Life Science, School of Chemistry and Chemical Engineering, Chemistry and Biomedicine Innovation Center (ChemBIC), Nanjing University, Nanjing, Jiangsu 210023, China;* orcid.org/0000-0003-0870-7142; Email: weihui@nju.edu.cn

Authors

Yufeng Liu − *Department of Biomedical Engineering, College of Engineering and Applied Sciences, Nanjing National Laboratory of Microstructures, Jiangsu Key Laboratory of Artificial Functional Materials, Nanjing University, Nanjing, Jiangsu 210023, China;* orcid.org/0000-0002-2355-4706

Xiaoyu Wang − *Department of Biomedical Engineering, College of Engineering and Applied Sciences, Nanjing National Laboratory of Microstructures, Jiangsu Key Laboratory of Artificial Functional Materials, Nanjing University, Nanjing, Jiangsu 210023, China;* orcid.org/0000-0002-8641-2430

Quan Wang − *Department of Biomedical Engineering, College of Engineering and Applied Sciences, Nanjing National Laboratory of Microstructures, Jiangsu Key Laboratory of Artificial Functional Materials, Nanjing University, Nanjing, Jiangsu 210023, China*

Yihong Zhang − *Department of Biomedical Engineering, College of Engineering and Applied Sciences, Nanjing National Laboratory of Microstructures, Jiangsu Key Laboratory of Artificial Functional Materials, Nanjing University, Nanjing, Jiangsu 210023, China*

Quanyi Liu − *State Key Laboratory of Electroanalytical Chemistry, Changchun Institute of Applied Chemistry, Chinese Academy of Science, Changchun, Jilin 130022, China*

Shujie Liu − *Department of Biomedical Engineering, College of Engineering and Applied Sciences, Nanjing National Laboratory of Microstructures, Jiangsu Key Laboratory of Artificial Functional Materials, Nanjing University, Nanjing, Jiangsu 210023, China*

Sirong Li − *Department of Biomedical Engineering, College of Engineering and Applied Sciences, Nanjing National Laboratory of Microstructures, Jiangsu Key Laboratory of Artificial Functional Materials, Nanjing University, Nanjing, Jiangsu 210023, China*

Yan Du − *State Key Laboratory of Electroanalytical Chemistry, Changchun Institute of Applied Chemistry, Chinese Academy of Science, Changchun, Jilin 130022, China;* orcid.org/0000-0003-3197-7204

Complete contact information is available at: https://pubs.acs.org/10.1021/acs.analchem.1c03610

Notes

The authors declare no competing financial interest.

■ ACKNOWLEDGMENTS

The authors thank Prof. Hang Xing for the analysis of MOF structure. This work was supported by National Natural Science Foundation of China (21874067), the National Key R&D Program of China (2019YFA0709200), Postdoctoral Research Funding of Jiangsu Province (2021K392C), CAS Interdisciplinary Innovation Team (JCTD-2020-08), PAPD Program, and Fundamental Research Funds for the Central Universities (021314380195).

■ REFERENCES

(1) Hanson, A. D.; McCarty, D. R.; Henry, C. S.; Xian, X.; Joshi, J.; Patterson, J. A.; Garcia-Garcia, J. D.; Fleischmann, S. D.; Tivendale, N. D.; Millar, A. H. *Proc. Natl. Acad. Sci. U.S.A.* **2021**, *118*, No. e2023348118.

(2) Rodrigues, R. C.; Ortiz, C.; Berenguer-Murcia, A.; Torres, R.; Fernandez-Lafuente, R. *Chem. Soc. Rev.* **2013**, *42*, 6290−6307.

(3) Varadarajan, N.; Gam, J.; Olsen, M. J.; Georgiou, G.; Iverson, B. L. *Proc. Natl. Acad. Sci. U.S.A.* **2005**, *102*, 6855−6860.

(4) Lancaster, L.; Abdallah, W.; Banta, S.; Wheeldon, I. *Chem. Soc. Rev.* **2018**, *47*, 5177−5186.

(5) Huang, Y.; Ren, J.; Qu, X. *Chem. Rev.* **2019**, *119*, 4357−4412.

(6) Liang, M.; Yan, X. *Acc. Chem. Res.* **2019**, *52*, 2190−2200.

(7) Wu, J.; Wang, X.; Wang, Q.; Lou, Z.; Li, S.; Zhu, Y.; Qin, L.; Wei, H. *Chem. Soc. Rev.* **2019**, *48*, 1004−1076.

(8) Huang, L.; Chen, J.; Gan, L.; Wang, J.; Dong, S. *Sci. Adv.* **2019**, *5*, No. eaav5490.

(9) Wei, H.; Gao, L.; Fan, K.; Liu, J.; He, J.; Qu, X.; Dong, S.; Wang, E.; Yan, X. *Nano Today* **2021**, *40*, No. 101269.

(10) Manea, F.; Houillon, F. B.; Pasquato, L.; Scrimin, P. *Angew. Chem., Int. Ed.* **2004**, *43*, 6165−6169.

(11) Zaramella, D.; Scrimin, P.; Prins, L. J. *J. Am. Chem. Soc.* **2012**, *134*, 8396−8399.

(12) Wulff, G. *Chem. Rev.* **2002**, *102*, 1−27.

(13) Zhou, Y.; Sun, H.; Xu, H.; Matysiak, S.; Ren, J.; Qu, X. *Angew. Chem., Int. Ed.* **2018**, *57*, 16791−16795.

(14) Zhang, Z.; Zhang, X.; Liu, B.; Liu, J. *J. Am. Chem. Soc.* **2017**, *139*, 5412−5419.

(15) Nath, I.; Chakraborty, J.; Verpoort, F. *Chem. Soc. Rev.* **2016**, *45*, 4127−4170.

(16) Lu, W.; Wei, Z.; Gu, Z.-Y.; Liu, T.-F.; Park, J.; Park, J.; Tian, J.; Zhang, M.; Zhang, Q.; Gentle, T., III; Bosch, M.; Zhou, H.-C. *Chem. Soc. Rev.* **2014**, *43*, 5561−5593.
(17) Shi, W.; Cao, L.; Zhang, H.; Zhou, X.; An, B.; Lin, Z.; Dai, R.; Li, J.; Wang, C.; Lin, W. *Angew. Chem., Int. Ed.* **2017**, *56*, 9704−9709.
(18) Li, M.; Chen, J.; Wu, W.; Fang, Y.; Dong, S. *J. Am. Chem. Soc.* **2020**, *142*, 15569−15574.
(19) Zhang, P.; Sun, D.; Cho, A.; Weon, S.; Lee, S.; Lee, J.; Han, J. W.; Kim, D.-P.; Choi, W. *Nat. Commun.* **2019**, *10*, No. 940.
(20) Liu, Y.; Zhou, M.; Cao, W.; Wang, X.; Wang, Q.; Li, S.; Wei, H. *Anal. Chem.* **2019**, *91*, 8170−8175.
(21) Zhang, J.; Liu, J. *Nanoscale* **2020**, *12*, 2914−2923.
(22) Liu, Y.; Wang, X.; Wei, H. *Analyst* **2020**, *145*, 4388−4397.
(23) Yang, H.; Xu, B.; Li, S.; Wu, Q.; Lu, M.; Han, A.; Liu, H. *Small* **2021**, *17*, No. 2007090.
(24) Cheng, H.; Liu, Y.; Hu, Y.; Ding, Y.; Lin, S.; Cao, W.; Wang, Q.; Wu, J.; Muhammad, F.; Zhao, X.; Zhao, D.; Li, Z.; Xing, H.; Wei, H. *Anal. Chem.* **2017**, *89*, 11552−11559.
(25) Zhang, W.; Lu, G.; Cui, C.; Liu, Y.; Li, S.; Yan, W.; Xing, C.; Chi, Y. R.; Yang, Y.; Huo, F. *Adv. Mater.* **2014**, *26*, 4056−4060.
(26) Zhao, M.; Wang, Y.; Ma, Q.; Huang, Y.; Zhang, X.; Ping, J.; Zhang, Z.; Lu, Q.; Yu, Y.; Xu, H.; Zhao, Y.; Zhang, H. *Adv. Mater.* **2015**, *27*, 7372−7378.
(27) Li, S.; Hou, Y.; Chen, Q.; Zhang, X.; Cao, H.; Huang, Y. *ACS Appl. Mater. Interfaces* **2020**, *12*, 2581−2590.
(28) Meng, Y.; Li, W.; Pan, X.; Gadd, G. M. *Environ. Sci. Nano* **2020**, *7*, 1305−1318.
(29) Jiao, L.; Yan, H.; Wu, Y.; Gu, W.; Zhu, C.; Du, D.; Lin, Y. *Angew. Chem., Int. Ed.* **2020**, *59*, 2565−2576.
(30) Pedone, D.; Moglianetti, M.; Lettieri, M.; Marrazza, G.; Pompa, P. P. *Anal. Chem.* **2020**, *92*, 8660−8664.
(31) Jia, H.; Yang, D.; Han, X.; Cai, J.; Liu, H.; He, W. *Nanoscale* **2016**, *8*, 5938−5945.
(32) Lou, Z.; Zhao, S.; Wang, Q.; Wei, H. *Anal. Chem.* **2019**, *91*, 15267−15274.
(33) Wang, X.-N.; Li, J.-L.; Zhao, Y.-M.; Pang, J.; Li, B.; Zhang, T.-L.; Zhou, H.-C. *Chem. Commun.* **2019**, *55*, 6527−6530.

https://doi.org/10.1021/acs.analchem.1c03610
Anal. Chem. 2021, 93, 15150−15158